Real-Time Load and Ancillary Support for a Remote Island Power System Using Electric Boats

Mahmud, K.; Rahman, M. S.; Ravishankar, J.; Hossain, J.; Guerrero, J. M.

Published in:
IEEE Transactions on Industrial Informatics

DOI (link to publication from Publisher):
10.1109/TII.2019.2926511

Publication date:
2020

Document Version
Accepted author manuscript, peer reviewed version

This article has been accepted for publication in a future issue of this journal, but has not been fully edited. Content may change prior to final publication. Citation information: DOI 10.1109/TII.2019.2926511, IEEE Transactions on Industrial Informatics

Real-Time Load and Ancillary Support for a Remote Island Power System Using Electric Boats

Khizir Mahmud, Md. Shamiur Rahman, *Student Member, IEEE*, Jayashri Ravishankar, MJ Hossain, *Senior Member*, *IEEE*, Josep M. Guerrero, *Fellow, IEEE*

***Abstract*--Powering small islands with reliable, affordable and green electricity is a big challenge due to their dispersed geographical location with limited number of consumers and the heavy dependence on fossil fuels. This paper aims to address this challenge of reducing dependency on fossil fuel generators by providing an easy and feasible solution using available and accessible energy resources. The proposed method utilizes the bidirectional energy transfer mechanism available in electric boats to support the consumers' power demand. It proposes a new real-time load-support (RTLS) system with a coordinated control using electric boats (EBs), community generators and battery energy-storage systems. It analyzes the management of the intermittent sources-dependent small-scale grid in real time, under various weather, load, and battery state-of-charge conditions. The RTLS system coordinates the customers' load demand with the available EBs, photovoltaics (PVs) and battery storage to provide efficient load support and to regulate the bus voltage and frequency. The efficacy of the proposed system is validated both computationally in a real network and in a laboratory setup. It is found that this novel system can substantially reduce the grid load demand and maintain the power quality under various load/source uncertainties and fault conditions. The system robustness is also evaluated considering undesirable conditions, such as severe three-phase faults and sudden EB disconnections. The performance of the proposed method is compared with that of the day-ahead load-management approach to validate its effectiveness under various scenarios.**

***Index Terms*-- Ancillary support, electric boat, forecasting, island energy management, island power systems, load support.**

NOMENCLATURE

pv_c^i	single PV module capacity
η_5	efficiency of PV module
$\eta_1, \eta_2, \eta_3, \eta_4$	efficiency of converter 1, 2, 3, 4
i_{pv}	current from PV
i_{eb}, i_b	current from EB and battery respectively
p_{pv}^g	amount of power supplied from PV to AC bus
p_{pv}^b	amount of power supplied from PV to fixed battery
c_{eb}^c	EB battery capacity
c_b^c	fixed battery capacity
c_{eb}^{max}, c_b^{max}	max. charging limit of the EB and battery respectively
c_{eb}^{min}, c_b^{min}	min. discharging limit of the EB and battery respectively
c_{eb}^i, c_b^i	SOC of the EB and battery at a particular (i^{th}) time

Khizir Mahmud and Jayashri Ravishankar are with the School of Electrical Engineering and Telecommunications, University of New South Wales, NSW 2052, Australia, email: (khizir.mahmud@unsw.edu.au, jayashri.ravishankar@unsw.edu.au).

Md Shamiur Rahman is with the ElectraNet Pty Ltd, SA 5000, Australia, email: (md-shamiur.rahman@students.mq.edu.au).

MJ Hossain is with the School of Engineering, Macquarie University, NSW 2109, Australia, email: (jahangir.hossain@mq.edu.au).

Josep M. Guerrero is with the Department of Energy Technology, Aalborg University, 9220 Aalborg East, Denmark. Email: (joz@et.aau.dk).

I. INTRODUCTION

THE past decade has experienced a rapid improvement in power systems, from generation and distribution to monitoring and power-quality equipment. Some well-known examples of this improvement are intelligent power-system stabilizers, advanced generator spinning reserves, and the availability of customer-level power-factor correction (PFC) devices [1]. These have led to a decline in the risk of a grid's instability, reliability and power-quality issues. However, for small-scale power grids, especially islanded microgrids, for instance in small geographical islands, power quality, stability, reliability, and load-shedding issues are still challenging issues. Both financial and technical aspects are known to be the underlying constituents associated with these factors [1]. Usually, the owner of a small-island community generator and the customers are reluctant to invest in power-quality insurance appliances. On the contrary, lack of a grid's inertia, generator spinning reserve, and quicker dynamic response are significant contributory factors to the technical challenges [1].

A holistic scenario of a small-scale power system indicates a growing trend towards the deployment of renewable-energy sources like roof-top photovoltaics (PVs) [1]. However, as the output power of PV units is highly dependent on sunlight, they are intermittent and non-dispatchable. Moreover, excess PV power generation during the middle of the day in off-peak hours introduces over-voltage problems in power systems. Therefore, unregulated high penetration of PV units can affect the reliability of the grid [2]. Furthermore, the lack of spinning reserve of these small generators may trigger an instability in power grids [3]. Additionally, these inverter-based generators have a quicker dynamic response than the conventional rotating machines, and this may cause oscillation which can result in network disturbances [4].

Recently, there has been renewed interest in battery storage in both stationary and mobile installations. A significant and growing body of stationary-battery installation has gained momentum in various scales and levels of the grid, e.g. small-scale roof-top PV-attached battery, or grid-side large-scale battery storage [1, 3]. Likewise, the batteries in electric vehicles (EVs) have been attracting a lot of interest owing to the bidirectional vehicle-to-grid (V2G) energy transfer mechanism. Although EVs are not available on a remote island, a similar bidirectional energy transfer mechanism in other types of storage could be a contributing factor to the power quality and load support to the grid, e.g. electric boats (EBs). An EB works similar to an EV, however, there is a fundamental difference in their design and functionalities. The installation of renewables like PVs and wind power at EBs facilitate them to charge their batteries and make their power less intermittent, unlike EVs. Additionally, a towed generator or a free-wheeling drive

This article has been accepted for publication in a future issue of this journal, but has not been fully edited. Content may change prior to final publication. Citation information: DOI 10.1109/TII.2019.2926511, IEEE Transactions on Industrial Informatics

propeller during sailing or normal operation can charge its battery [5, 6]. Therefore, unlike EVs, an EB can provide power to the grid even immediately after coming from a trip. Although having a vast potential, surprisingly little attention has been paid to utilize EBs to resolve the power crisis of a remote island.

Numerous studies [7-9] are conducted to explain the basic properties and challenges of a remote island power system. The use of renewable-energy sources is a well-established approach to manage customers' energy demand [10, 11]. The most common renewable-energy sources (RESs) are photovoltaics, wind power, and micro-hydro. These RESs are utilized in various ranges and scales using different control methods. The authors in [10] adopted a multi-time-scale scheduling framework to manage the renewable-energy penetration in a small-scale island power system. A different approach to RES penetration uses active network management to monitor and control the power generation in real time and schedules the flexible demands. Two-stage stochastic optimization and scheduling techniques are investigated [12] to manage the intermittent wind-power penetration in a small island. Authors in [13, 14] develop a dispatch method for roof-top and aggregated PV units to tackle the power shortage and power-quality issues. An intelligent load-shedding strategy is proposed in [11] using a unique protection system to prevent the tripping of a diesel generator due to the intermittency in PV units. The developed system [11] detects the amount of power-output reduction of a PV unit, and the special protection system executes the load interruption. However, the fundamental goal of an uninterrupted power supply to customers is understudied. A reasonable approach to tackle this issue could be renewable-energy generation prediction [14] and hour-ahead management. So far, however, there has been little discussion about the impact of the prediction errors in these volatile generators and their compensation challenges.

A systematic understanding of how an hour-ahead prediction and management contributes to an uninterrupted power supply to customers is still lacking. A wind-power-based power-support system [15, 16] is another popular mode to provide a power supply to a small island community. In some cases [17], pumped hydro in combination with renewable-energy sources are also used. Again, the uncertainty, prediction error and time-ahead management remain a question. A great deal of previous research [18, 19] into hybrid microgrids has focused on the use of PV units, battery-energy-storage systems and fuel cells in various combinations to provide load support. A considerable amount of research [20, 21] are conducted to mitigate the intermittency problem of wind and PV power generation systems using battery energy storage systems. Various control approaches, such as a model predictive control strategy [20], droop control [22], preventive control strategy [23], and optimization methods like generic algorithms [21] are used to enhance renewable-energy penetration. Additionally, over and under-voltage protection, under-frequency control, and prevention of diesel-generator tripping due to under-frequency of the system are also discussed. However, the complete dependence on battery-energy-storage systems for power quality and load support indicates a need for over-capacity battery installation, which is a costly solution for an island community. The burden of battery storage and the overall installation cost can be minimized if an existing resource such as an electric boat (EB) can be included in the system. The idea of utilizing EBs to meet small-island power demand and improve power quality is emerging and requires further studies to analyze their feasibility. Previous researches on EBs [5, 6] has been mostly focused to improve internal functionalities; such as internal energy management, diesel-generator control, renewable-energy integration, and conduct economic analysis of hybrid EBs. A systematic and through analysis is required to critically investigate its feasibility and impacts to provide load and ancillary support in a small-island energy-management system which is not available. The charge-discharge management of EBs to provide load and ancillary support are also not discussed clearly in existing literature. Likewise, the mitigation of PV intermittency using EBs in real weather, load and uncertainty conditions remains unclear.

This paper provides a first comprehensive investigation to utilize EBs for load and ancillary support of a remote island power system. A robust control algorithm is developed and tested in a real network. Real-time load and weather conditions are considered to evaluate the performance of the designed control system. Additionally, a charge-scheduling algorithm for both the battery and the electric boat are developed. The performance of the proposed approach is compared with that of artificial neural networks (ANNs) and tested via laboratory experiments. In summary the contribution of this paper is to:

- investigate the feasibility of an electric boat as a noble element to provide load and ancillary services to small island power systems;
- develop a new charging-discharging algorithm for electric boats which can provide excellent ancillary services to the grid;
- design and implement a coordination control algorithm for the available energy resources (i.e. EBs, PV units and battery storages) based on factors like load conditions, storage state-of-charge (SOC), and generate a coordinated response for load and ancillary support;
- apply an accurate prediction technique for the management of the energy generation and customers' power demand in real-time load and weather conditions on a real network;
- develop a robust energy management system resilient to load and power generation uncertainty and severe faults;
- compare the performance of the proposed system with an ANN-based energy management system; and
- verify the performance of the proposed system in a laboratory prototype system with a smaller capacity.

The remaining part of the paper is structured as follows. Section II provides an overview of the proposed system with a comprehensive and pictorial representation of its architecture. Section III details the algorithm. The performance of the proposed system is tested through various case studies in Section IV. Section V presents the experimental results followed by the conclusion in Section VI.

II. System Overview

In this paper, a community-based load-support system for a small island is proposed using existing resources, such as electric boats (EB), photovoltaics (PVs) and battery-energy-storage systems. The power from the aggregated EBs are utilized using the proposed bidirectional boat-to-grid (B2G) technique. A cluster of PV cells associated with a small capacity of battery storage is also considered in the system. All

This article has been accepted for publication in a future issue of this journal, but has not been fully edited. Content may change prior to final publication. Citation information: DOI 10.1109/TII.2019.2926511, IEEE Transactions on Industrial Informatics

these energy resources are integrated to a common bus from which the individual customers receive power. A controller, associated with converters, EBs, PVs, and battery storage, controls the power flow from/to EBs and battery storages. A detailed schematic of the proposed system is illustrated in Figure 1 [27].

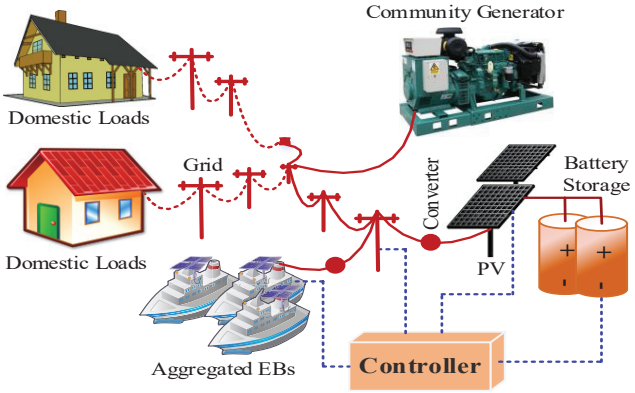

Fig. 1. Overview of the proposed system

A more comprehensive architectural detail of the proposed system is illustrated in Figure 2 [27]. Aggregated EBs, PVs, and battery-energy-storage systems are connected to a common AC bus. The PV cells are connected to the DC bus through a converter 1 (unidirectional dc-dc converter). The excess energy from PV during off-peak hours is bypassed to the battery through converter 2 (bidirectional dc-dc converter). The battery charges and discharges through this converter. The bidirectional energy transactions between DC and AC bus are conducted using converter 3, which is a bidirectional DC-AC/AC-DC converter. The converter 4 is another bidirectional DC-AC/AC-DC converter which enables the energy transfer from/to grid/boat. The controller reads the grid load conditions, SOC of the battery, SOC of the electric boat (EB), and the PV power generation. Based on these variables, the controller operates the converter to control battery charging/discharging.

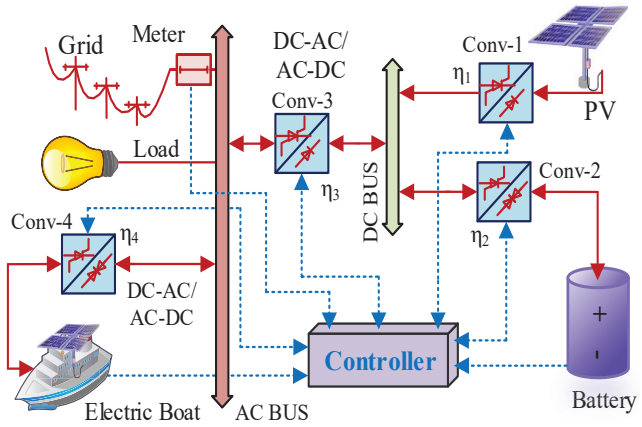

Fig. 2. A comprehensive view of the proposed architecture.

III. Proposed Approach

While some research has been carried out to provide load support and resolve power-quality issues in a small island [15-16, 18-19], there is still very little understanding of an EB's integration to a small-scale grid to provide load and power-quality support. The coordinated control strategy adopted in this paper, for the first time, will contribute to a deeper understanding of the load and ancillary support mechanism using EBs. The grid load curve is formulated as a function of power and time. This grid load demand at a particular bus is the summation of the total power demand of the customers connected to that bus. The voltage at the common AC bus remains constant, so the current varies based on the consumers' power demand. The load curve considered as a function of power and time is as follows [27]:

$$l_t^p = f(p,t) \tag{1}$$

Assume that the customers' desired base-load demand is

$$l_{t,b}^p = f(p_b,t_b) \tag{2}$$

Charging and discharging of the battery and EB is controlled based on the off-peak and peak load periods. The frequency of the charge-discharge cycles is related to the battery lifecycle. The load condition (peak/off-peak) is read by the controller in a sub-second time scale. Peak and off-peak load may occur several times in a day or a week, or within a particular duration. Let assume each time, the off-peak load (base-load) initiates at t_b^i, and stops at t_b^s, whereas the peak load initiates at t_p^i and stops at t_p^s. The base-load duration is expressed as:

$$t_b^d = \{t_b^i, (t_b^i+1), (t_b^i+2), \ldots\ldots, t_b^s\} \tag{3}$$

Likewise, the duration of peak load occurrence period is expressed as:

$$t_p^d = \{t_p^i, (t_p^i+1), (t_p^i+2), \ldots\ldots, t_p^s\} \tag{4}$$

The time (t) in (1) is the combination of both the peak and off-peak load periods, i.e.

$$t = \sum (t_b^d, t_p^d) \tag{5}$$

The difference between two data reading points (with respect to time), i.e. $\{(t_b^i+1)-t_b^i\}$ and $\{(t_p^i+1)-t_p^i\}$ defines the data acquisition rate by the controller which is done in a sub-second time scale. The power demand $(p), p \in l_t^p$, whether peak or off-peak are identified as below.

$$(l_t^p - l_{t,b}^p)\begin{cases} positive\ for\ peak\ power\ demand \\ negative\ for\ off-peak\ power\ demand \end{cases} \tag{6}$$

For $(l_t^p < l_{t,b}^p)$ at any i^{th} time the amount of power available to charge EB and battery is

$$p_a = \{l_{t,b}^p - l_t^p\}, p_a \geq 0 \tag{7}$$

This available power will be allocated between EB and battery

$$p_a = \underbrace{p_a^b}_{battery} + \underbrace{p_a^{eb}}_{EB} \tag{8}$$

Here, p_a^b and p_a^{eb} are the maximum available power to charge battery and EB respectively. If the SOC of the battery at the i^{th} time is c_b^i (in percent), and the maximum charging limit of the battery is c_b^{max} (in percentage), the required energy to charge the battery is

$$p_r^b = \{(c_b^{max} - c_b^i) * c_b^c\} * \eta_2;\ p_r^b \leq p_a^b \tag{9}$$

Here c_b^c is the battery capacity. The required energy p_r^b will be met from the available grid power p_a^b. If the battery does not require energy, then $p_r^b = 0$. For the EB, the required energy is a function of the current and the desired SOC, as the terminal voltage remains constant. Assuming that the instantaneous SOC of an EB at the i^{th} time is c_{eb}^i (in percent), and the maximum charging limit set by the owner is c_{eb}^{max} (in percentage), the required energy to charge the EB is

$$p_r^{eb} = \{(c_{eb}^{max} - c_{eb}^i) * c_{eb}^c\} * \eta_4;\ p_r^{eb} \leq p_a^{eb} \tag{10}$$

This article has been accepted for publication in a future issue of this journal, but has not been fully edited. Content may change prior to final publication. Citation information: DOI 10.1109/TII.2019.2926511, IEEE Transactions on Industrial Informatics

$$(p_r^b + p_r^{eb}) \leq p_a \tag{11}$$

Here c_{eb}^c is the EB battery capacity. The required energy p_r^{eb} will be met from the available grid power p_a^{eb}. According to the system, PV power is shared between the common AC bus (through intermediate DC bus) and the battery. If $l_t^p > l_{t,b}^p$, all PV power is supplied to the common AC bus. The amount of supplied power is

$$p_{pv}^g = n(pv_c^i * \eta_5) * \eta_1 \tag{12}$$

If $l_t^p < l_{t,b}^p$, PV power is bypassed through converter 2 and shared between the AC bus and the battery. The amount of power to the battery at the i^{th} time for $(l_t^p < l_{t,b}^p)$ is

$$p_{pv}^b = \left[l_t^p - \{n(pv_c^i * \eta_1)\}\right] * \eta_2 \tag{13}$$

For $\left(l_t^p > l_{t,b}^p\right)$ at any i^{th} time the amount of power required to provide the domestic power demand support is

$$p_d^l = \{l_t^p - l_{t,b}^p\}, p_d^l \geq 0 \tag{14}$$

This required power will be requested from the EB, battery and PV, and their individual amount is expressed as:

$$p_d^l = \underbrace{p_{d,l}^b}_{battery} + \underbrace{p_{d,l}^{eb}}_{EB} + \underbrace{p_{pv}^g}_{PV} \tag{15}$$

Here, $p_{d,l}^b$ and $p_{d,l}^{eb}$ are the maximum power that are required to be discharged from the available energy from the battery and EB respectively. If the EB is not available at any particular time, then $p_{d,l}^{eb} = 0$. Any shortage or unavailability of the requested power is met by the community generator. The power that will be provided by the community generator during peak load hours is

$$\underbrace{p_{c,g}^p}_{\substack{community\\ generator}} = \underbrace{l_t^p}_{\substack{power\\ demand}} - \underbrace{\{p_{d,l}^b + p_{d,l}^{eb} + p_{pv}^g\}}_{\substack{power\ from\\ PV,EB,battery}} \tag{16}$$

If the minimum SOC level that the battery and EB are allowed to discharge are c_b^{min} and c_{eb}^{min} respectively, the maximum energy that the battery and EB can discharge to meet the requested power is

$$p_{en}^b = \{(c_b^i - c_b^{min}) * c_b^c\} * \eta_2 * \eta_3 \tag{17}$$

$$p_{en}^{eb} = \{(c_{eb}^i - c_{eb}^{min}) * c_{eb}^c\} * \eta_4 \tag{18}$$

Here, p_{en}^b and p_{en}^{eb} are the maximum dischargeable energy at i^{th} time by the battery storage and EB, respectively. This maximum energy by the battery storage and EB will be provided to respond the requested power, i.e. $p_{en}^b \rightarrow p_{d,l}^b$ and $p_{en}^{eb} \rightarrow p_{d,l}^{eb}$. The discharging or charging of the battery at a particular time is identified by the polarity of the current, i.e.

$$\forall i \in f(l_t^p, t) = \begin{cases} i_{eb}, i_b > 0 \; for \; l_t^p < l_{t,b}^p \\ i_{eb}, i_b < 0 \; for \; l_t^p > l_{t,b}^p \\ i_{pv} > 0 \; for \; (p_{pv}^g + p_{pv}^b) > 0 \\ i_{pv} = 0 \; for \; (p_{pv}^g + p_{pv}^b) = 0 \end{cases} \tag{19}$$

If the power demand of customers $\left(l_t^p\right)$ suddenly increases to $\left(\overline{\overline{l_t^p}}\right)$ under an uncertainty situation, the available resources (PV, EB, and battery) will try to meet the additional demand $\left(\overline{\overline{l_t^p}} - l_t^p\right)$. If their capacity is not enough then the spinning reserve $\left(\mathcal{S}_r^g\right)$ of the community generator will provide it.

$$\mathcal{S}_r^g = \overline{\overline{l_t^p}} - (p_{pv}^g + p_{d,l}^b + p_{d,l}^{eb}) \tag{20}$$

The sources and loads connected at the common AC bus at i^{th} time is identified as:

$$Sources \begin{cases} \underbrace{\left[\{(c_b^i - c_b^{min}) * c_b^c\} * \eta_2 * \eta_3\right]}_{battery} \\ \underbrace{\left[\{(c_{eb}^i - c_{eb}^{min}) * c_{eb}^c\} * \eta_4\right]}_{EB} \\ \underbrace{\left[n(pv_c^i * \eta_5) * \eta_3 * \eta_1\right]}_{PV} \end{cases} \tag{21}$$

$$Loads \begin{cases} \underbrace{l_t^p}_{household\ loads} \\ \underbrace{\left[\{(c_b^{max} - c_b^i) * c_b^c\} * \eta_2 * \eta_3\right]}_{battery} \\ \underbrace{\left[p_r^{eb} = \{(c_{eb}^{max} - c_{eb}^i) * c_{eb}^c\} * \eta_4\right]}_{EB} \end{cases} \tag{22}$$

The battery and EB charging-discharging constraints and their operational behavior using the proposed algorithm are shown in Figure 3. The charging-discharging rate based on the power demand of consumers, reference demand, upper and lower charging-discharging boundaries, battery capacity at a particular power demand and SOC condition are also depicted in this figure.

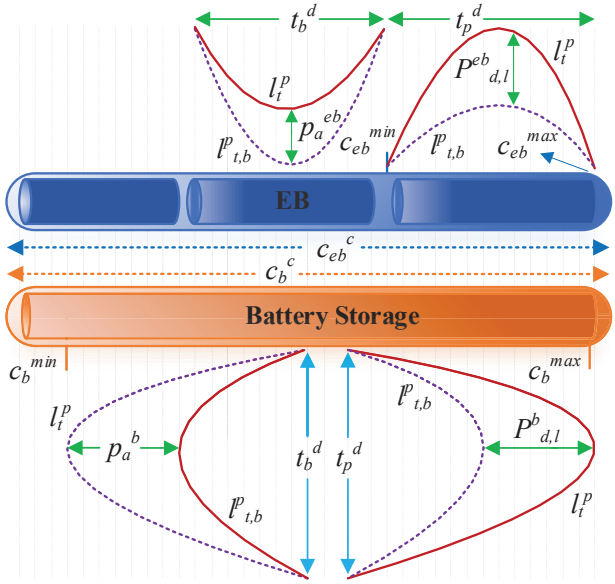

Fig. 3. Charging-discharging constraints of battery storage and EB.

A decentralized interfacing converter controller is utilized to interface the PV and EB to the load as shown in Figure 4 [19, 28]. It consists of two control loops for converter 3 and 4, i.e. a direct-quadrature reference current (i_{ld}^* and i_{lq}^*) generator loop and a current control loop [19, 24, 25, 28]. Initially, the AC-side voltage (v_o^{abc}) is fed to a phase-locked loop (PLL) to get an instantaneous angle measurement ($\tilde{\theta}$) which is later fed into an $(abc - dq0)$ converter. Then, v_o^{abc} and the inverter output current (i_l^{abc}) are passed through the $(abc - dq0)$ converter to get corresponding d and q axis components i.e. v_{od}, v_{oq}, i_{ld} and i_{lq}. The output active (P) and reactive power (Q) of the interfacing controller are controlled by i_{ld} and i_{lq} respectively. Both i_{ld} and i_{lq} need to follow their corresponding references to achieve desired control objectives. The measured P is compared with its reference P^*generated by (21). Later, the error signal $(P^* - P)$ is passed through a proportional-integral (PI)

This article has been accepted for publication in a future issue of this journal, but has not been fully edited. Content may change prior to final publication. Citation information: DOI 10.1109/TII.2019.2926511, IEEE Transactions on Industrial Informatics

controller to generate the control input i_{ld}^*. Similarly, the output reactive power (Q) of the inverter is compared with the reactive-power reference (Q^*), which is the load-reactive power demand. Later, the error is minimized using a PI controller by generating i_{lq}^* [19, 28].

The main task of the current-control loops is to compare i_{ld} and i_{lq} with their associated references i_{ld}^* and i_{lq}^* and decouple active and reactive power control. As a result, the controller performance becomes independent of the system dynamics [19, 24, 25, 28]. Finally, inverter voltage references v_{id}^* and v_{iq}^* are passed through a $(dq0 - abc)$ converter to generate modulation signal (v_{iabc}^*) that is fed to a PWM.

The upper part of Figure 4 shows the control of the DC-DC converter, i.e. converter 1 and 2. The PV voltage reference $\left(v_{pv}^{ref}\right)$ is generated from the tertiary controller in Figure 2, and compared with the measured DC voltage $\left(v_{pv}\right)$. The error is passed through the PI controller $\left(PI_{pv1}\right)$ keeping in mind that the current magnitude lies between the upper $\left(i_{lpv-max}\right)$ and lower $\left(i_{lpv-min}\right)$ range. The measured PV current $\left(i_{lpv}\right)$ is tracked with the reference current $\left(i_{pv}^*\right)$ generated from the outer PI controller with the help of inner PI controller $\left(PI_{pv2}\right)$ to generate the PWM. The same approach is applied to control the converter 2 except that the two switching PWM signal output for its bidirectional functionalities. In this case, the reference voltage signal, i.e. nominal DC-link voltage is $\left(v_{dc-ref}\right)$, measured voltage is (v_{dc}), reference current is (i_{lb}^*), measured current is (i_{lb}).

Gains of the PI controllers need to be tuned to ensure stable control operation. There are several well-established methods to optimize PI controllers in the literature [19], [26], [28]. Among them, the Ziegler–Nichols method has provided reasonable performance for tuning the PI controllers; thus, this method has been used in our system for optimizing purpose. Moreover, instead of using decentralized control framework, distributed or communication-assisted control can also be utilized if EBs are anchored in a distant manner [19]. However, EBs are considered to be anchored in a fixed place for this paper. Moreover, for the microgrids consisting of AC and DC bus, i.e. hybrid microgrids, selection of appropriate voltage levels and converter topologies are also important, which can be found in detail in [28].

A summary of the proposed RTLS system's design process is as follows:

Step I: Collect load condition data from smart meter, peak and off-peak load conditions, and the required load-support from sources (p_d^l), or available power (p_a) to charge storage using (1), (2), (7), (15).

Step II: Check PV power generation (p_{pv}^g) and check load conditions after getting power from PV units using (13) and (14).

Step III: Check battery SOC constraints c_b^i, c_b^{min}, c_b^{max}, c_b^c, and EB availability and EB SOC constraints c_{eb}^i, c_{eb}^{min}, c_{eb}^{max}, c_{eb}^c, and charge/discharge them from (p_a) and (p_d^l) based on the load status using (10- 12, 18-19).

Step IV: Generate P^* from (21) and Q^* from the measured reactive power demand at the load side.

Step V: Compare the active and reactive power tracking errors through PI controllers in order to generate i_{ld}^* and i_{lq}^* respectively for the current control loop.

Step VI: Utilize i_{ld}^* and i_{lq}^* in the decoupled current-control loop to generate reference v_{iabc}^*.

Step VII: Repeat the process until $|P^* - P| \& |Q^* - Q| \to 0$.

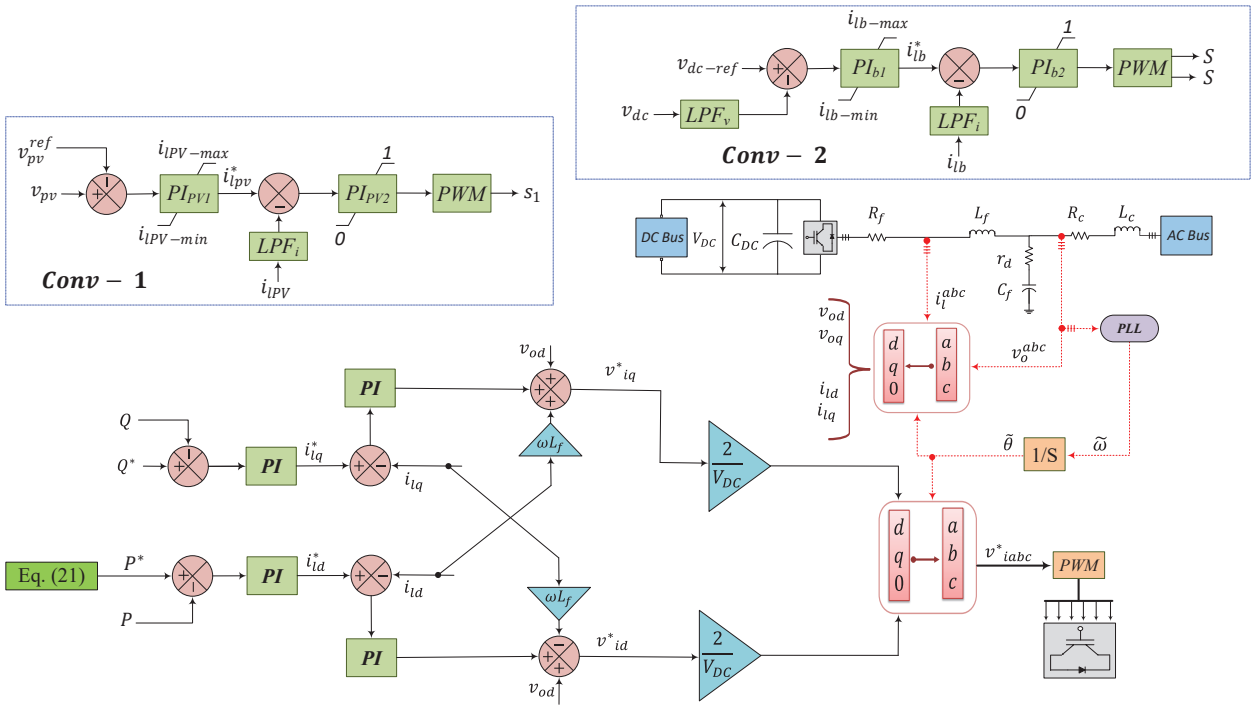

Fig. 4. Interfacing converter control structure.

This article has been accepted for publication in a future issue of this journal, but has not been fully edited. Content may change prior to final publication. Citation information: DOI 10.1109/TII.2019.2926511, IEEE Transactions on Industrial Informatics

IV. Case Studies

In this section several case studies on the proposed approach are conducted to verify its effectiveness. The specifications used for the analysis are listed in Table I.

TABLE I
Specifications used in the analysis

Components	Capacity
EB (1, 2, 3)	23, 24, 41 kWh
Battery storage	30 kWh
Battery SOC limit	30-98% SOC
EB SOC	Max. travel distance 40% of their SOC capacity
EB discharge limit	>30% SOC
PV Capacity	20 kW
Community Generator capacity	90 kVA max
EBs at work	8 am- 3 pm
Nominal AC bus voltage (RMS)	230- 240 V
PV inverter efficiency	90%
PV cell efficiency	13%

The power demand curves of the residents are shown in Figure 5. The residential load curves consist of a mix of constant impedance, constant current and constant power loads, and their basic proportions are approximately 27%, 41% and 32% respectively.

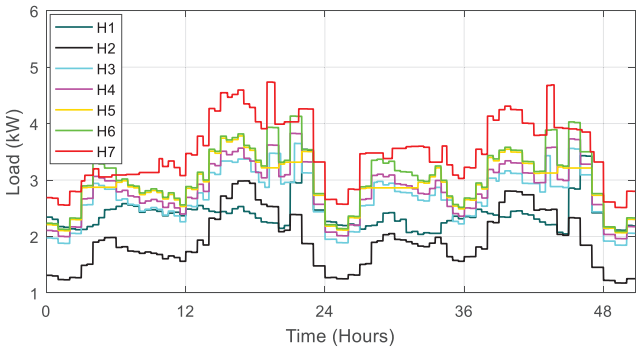

Fig. 5. Residents' load curves. 'H= House'.

A. Load-Support Analysis

This section discusses the load-support system using various combinations of EBs, PV units and battery-energy-storage systems. When a single EB is connected, the amount of load support is not significant because of the limited battery capacity, EB availability and the SOC limit as shown is Figure 6. However, the amount of load support increases with increasing number of EBs as set out in Figure 7.

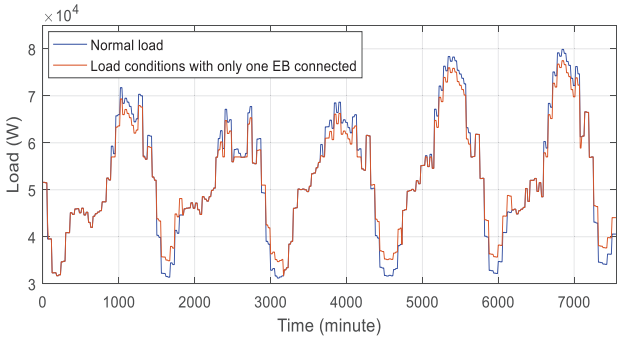

Fig. 6. Load-support condition when only one EB is connected.

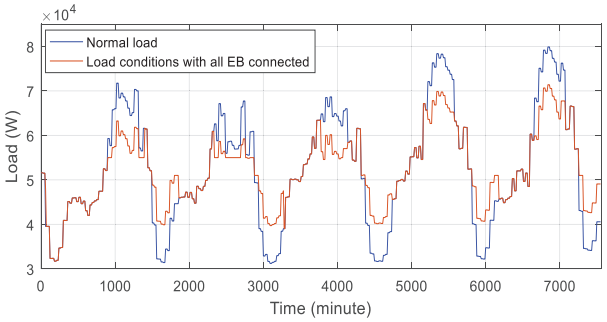

Fig. 7. Load-support condition when all 3 EBs are connected.

Integration of PVs without having any storage has a lesser significance to the consumers, as shown in Figure 8. This is because the PV power generation is maximum during mid-day and the load demand is less at that time. Therefore, any extra generation at lower demands may lead to over-voltage.

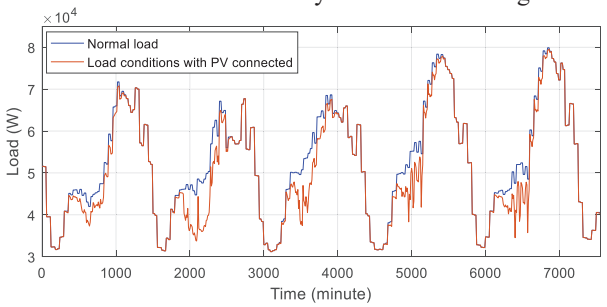

Fig. 8. Load-support condition when only PV is connected and no storage.

Storage support, either by a fixed battery or an EB can better utilize the power from the PV as shown in Figures 9 and 10. However, the only difference is the availability of the storage, since the capacity of a battery energy storage system is fixed and an EB is a mobile storage. The load support further increases if all the available resources are used, i.e. battery storage, all EBs and PV units, as in Figure 11.

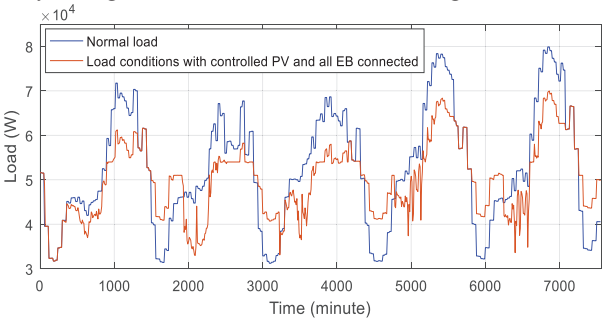

Fig. 9. Load-support condition with a PV and all EBs integration.

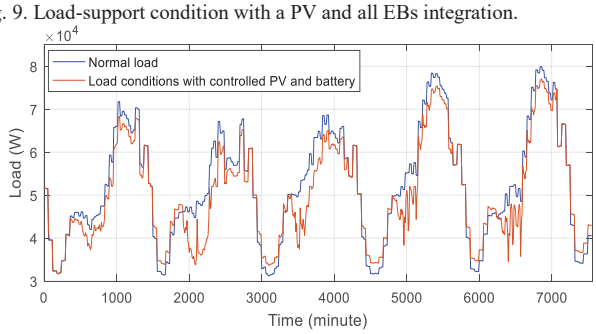

Fig. 10. Load-support condition with a PV and battery connection.

This article has been accepted for publication in a future issue of this journal, but has not been fully edited. Content may change prior to final publication. Citation information: DOI 10.1109/TII.2019.2926511, IEEE Transactions on Industrial Informatics

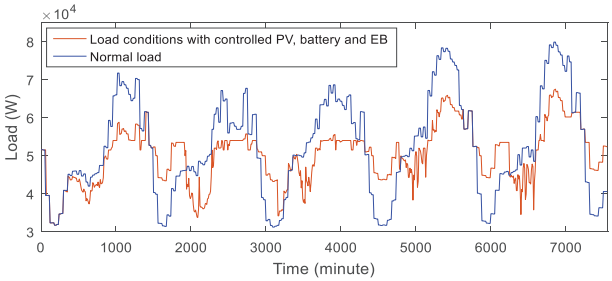

Fig. 11. Loads-support condition with all EB, PV and battery.

B. Impact of Load Uncertainty

This section investigates the robustness on the load-support system in case of uncertainty in the load. The system response is tested under ±15% load variation conditions. As can be seen from Figures 12 and 13, the load-support system is independent of load status. With a lower demand the percentage of peak-shaving is higher, whereas this percentage is lower for higher demand. However, the amount of load support remains the same.

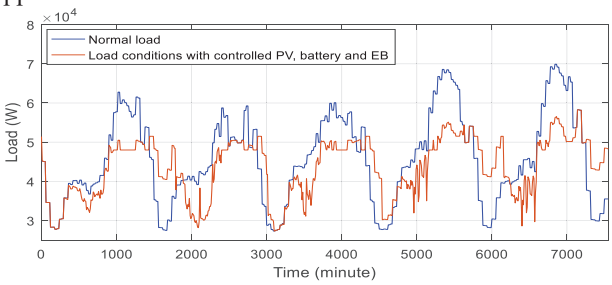

Fig. 12. Analysis of the load-support status in case of a 15% load decrement.

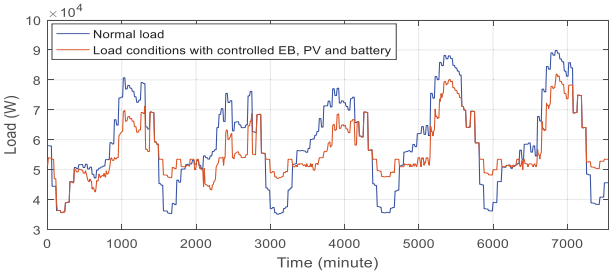

Fig. 13. Analysis of the load-support status in case of a 15% load increment.

C. Evaluation of System Robustness

The main objective of this section is to analyze the robustness of the system in terms of voltage and frequency regulation during and after undesirable operating conditions such as a three-phase fault or a sudden EB disconnection.

Case 1 (Normal islanded operation)

The performance of the proposed controller is evaluated in this case study considering normal islanded operation with variable PV generation and demand for one whole day. The generation and load profile are evenly distributed in 5 second simulation timeframes. The main objective of this case study is to validate the capability of the designed controller on system dynamics. From Figures 14 and 15, it is clear that both frequency and voltage are satisfactorily regulated with the proposed scheme in a variable PV power generation supported by a battery storage and an EB. The current condition at PCC in this case is shown in Figure 16.

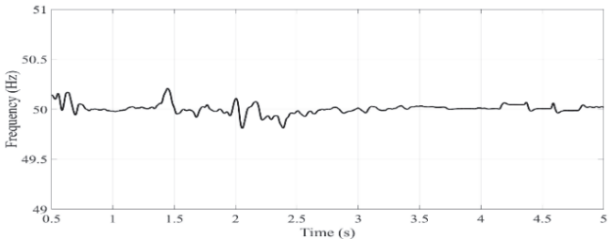

Fig. 14. Frequency of the system during normal operation.

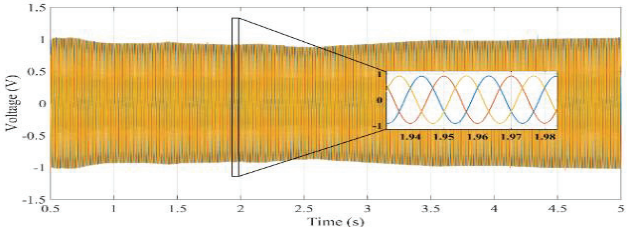

Fig. 15. PCC voltage in per unit (p. u.).

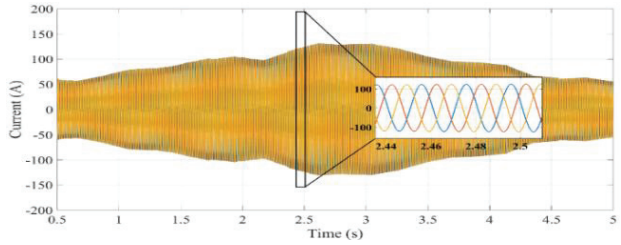

Fig. 16. PCC current.

Case 2 (Severe three-phase fault)

The main objective of this case study is to evaluate the fault ride-through capability of the system during and after a severe three-phase fault. The variable irradiation values, load profile and the simulation timeframe used in the previous case study are kept the same. At t = 2 s, a severe three-phase fault with a duration of 60 ms, which is equivalent to three cycles for a 50 Hz system, is applied at the point of common coupling (PCC). It can be observed that the system frequency experiences a fluctuation during that period (Figure 17); however, due to the robustness of the controller, under-voltage tripping is avoided. At t = 2.06 s the fault is cleared, and the PCC voltage returns to its nominal value at t = 2.15 s, as shown in Figure 18.

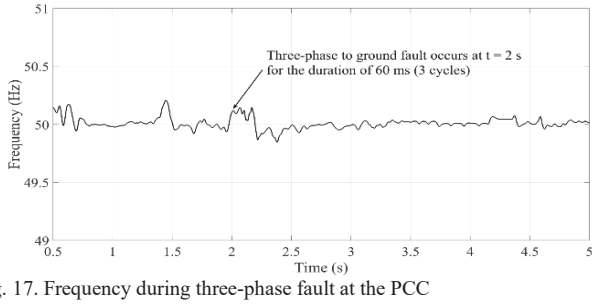

Fig. 17. Frequency during three-phase fault at the PCC

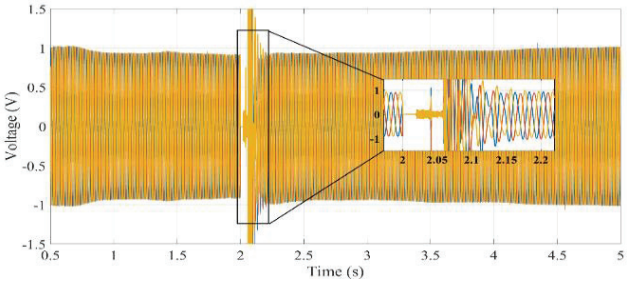

Fig. 18. PCC voltage in per unit (p. u.).

This article has been accepted for publication in a future issue of this journal, but has not been fully edited. Content may change prior to final publication. Citation information: DOI 10.1109/TII.2019.2926511, IEEE Transactions on Industrial Informatics

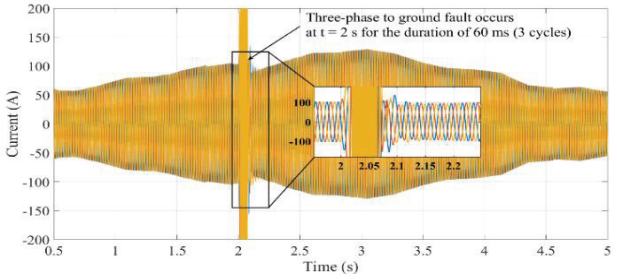

Fig. 19. PCC current.

Case 3 (Sudden EB disconnection)

EB owners should have the flexibility to withdraw their grid support at any time. In this case study, the effects of sudden disconnection of a high capacity EB on the system voltage and frequency is observed. Figure 20 shows the power curves of the battery and the EBs. At t = 2.5 s, one EB (EB-3) is intentionally disconnected. EB-3 is kept disconnected for the rest of the simulation period. In order to maintain stability of the system, other EBs react instantaneously based on their available capacities. It can be observed that, due to the simultaneous output-power sharing among available EB storages, the voltage and frequency of the system remain stable, as in Figures 21 and 22. Additionally, the current status under this case 3 is shown in Figure 23.

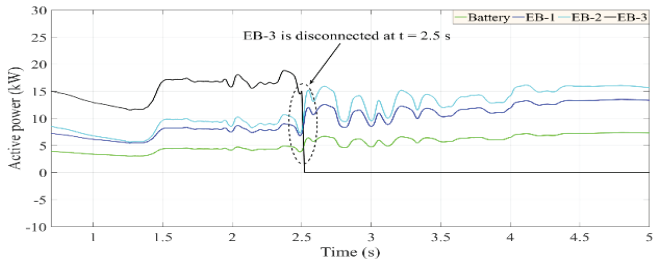

Fig. 20. Output power of PV, battery storages, and EBs during normal islanded operation.

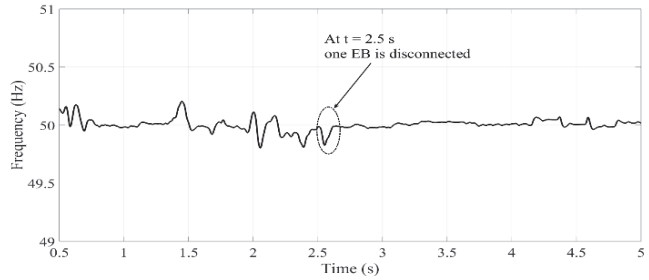

Fig. 21. Frequency of the system during normal operation.

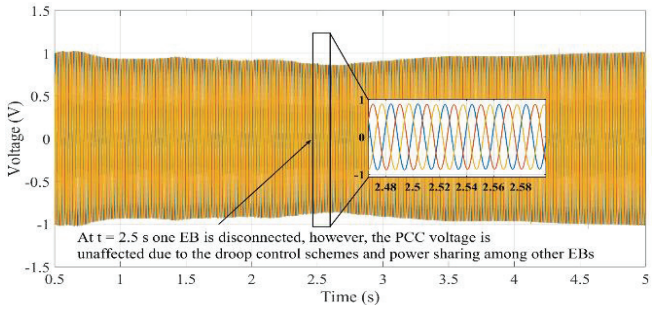

Fig. 22. PCC voltage in per unit (p. u.).

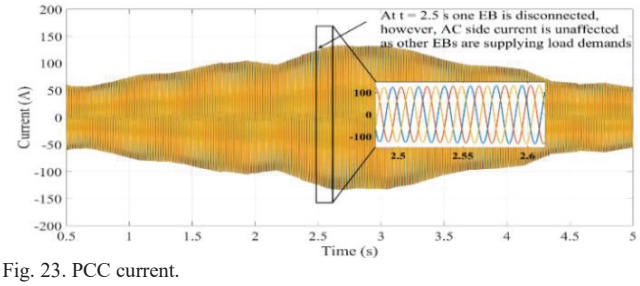

Fig. 23. PCC current.

The performance of the system under unbalanced load conditions are also investigated. A dynamic three-phase load having a different capacity at each phase is used to test the PCC voltage conditions, as shown in Figure 24.

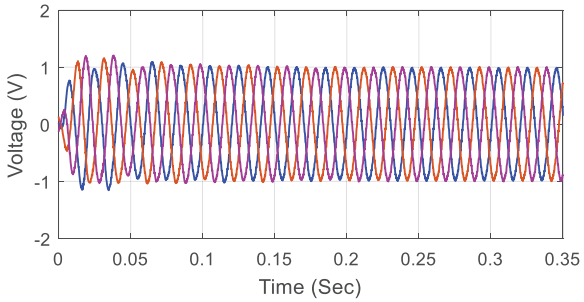

Fig. 24. PCC voltage in per unit (p. u.) during unbalanced load conditions.

The total harmonic distortion (THD) at the PCC is calculated to investigate the power quality status of the system. From the analysis it is found that the THD is below 5% which is in line with the IEEE 1547 standard. Detail of the THD status are shown in Figure 25.

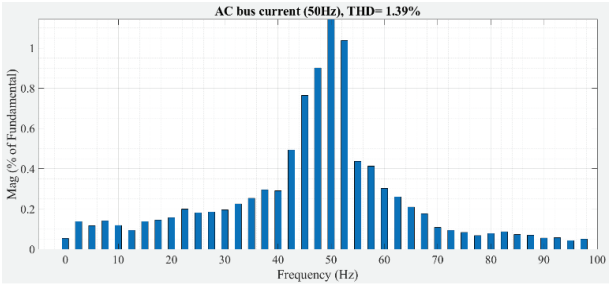

Fig. 25. THD at the PCC.

D. Comparison with ANN-Based Approach

This section shows a comparison between the proposed technique and the ANN-based load demand management approach as applied in [27]. ANN is useful for highly nonlinear applications and performs with less complexity and computational time [13]. 756 data set consisting of customers real power demand were used for training. Along with power demand, battery and EB SOC conditions and their constraints, EB availability, PV power generation data were also used to train the ANN network. During the training, validation and testing phases, various postprocessing analyses such as confusion matrix, error histogram and mean-square error were also investigated. The regression error in the training, validation, and testing stages is 0.913, 0.925 and 0.912, respectively. The overall error in all the stages is 0.915, and the best validation performance is found at epoch 29.

The comparison between the ANN and the proposed method is illustrated in Figure 26, and it is found that the

This article has been accepted for publication in a future issue of this journal, but has not been fully edited. Content may change prior to final publication. Citation information: DOI 10.1109/TII.2019.2926511, IEEE Transactions on Industrial Informatics

performance of the proposed method is quite similar to that of an ANN-based method; however, the proposed method is easier to implement.

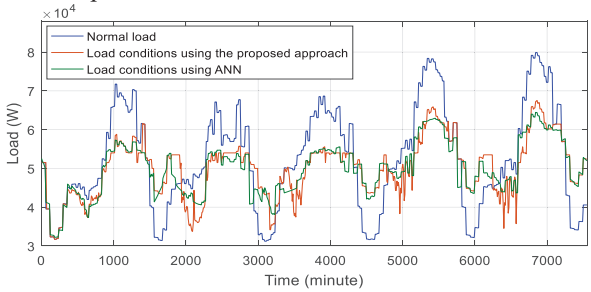

Fig. 26. Comparison of the proposed method with an ANN.

E. Real-Time Vs Day-Ahead Load-Support Approach

In this section, a day-ahead load-support system is modelled to show its performance in comparison to the real-time approach. An autoregressive moving average (ARMA) technique is used to predict the PV power generation, as shown in Figure 27, and the customers' load demand as shown in Figure 28. ARMA is the combination of the autoregressive (AR) and the moving average (MA), which maintains a linear relationship between its future variables and past observations and adds random errors and a constant. The ARMA model can be expressed as:

$$x_t = \sum_{i=1}^{p} \emptyset_i x_{t-1} + \zeta_t + \mathrm{Z} + \sum_{j=1}^{q} \partial_j \zeta_{t-j} \qquad (23)$$

where, x_t is the output from ARMA mode, p and q are the order of the model, $\emptyset_i$ and ∂_j are the model parameter, ζ_t is the random error, Z is a constant.

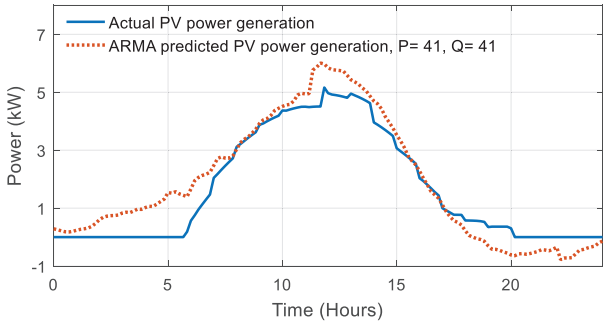

Fig. 27. PV power generation prediction using ARMA.

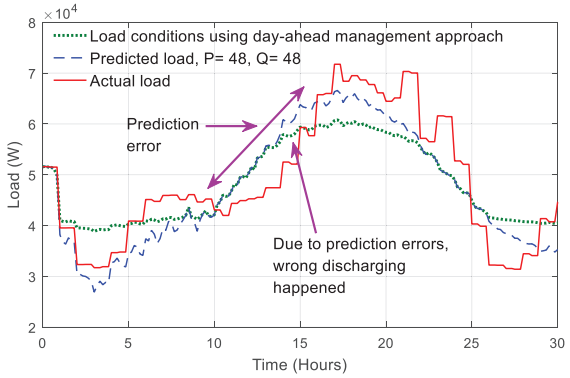

Fig. 28. Performance of the day-ahead load-support systems.

The case study conducted in Figure 10 is tested here using the ARMA-based predicted values. However, the investigation (in Figure 28) shows that due to the prediction errors, the battery storage charges and discharges at a wrong time, which does not function effectively to support the load and leads to inefficient cycling of storages.

F. EB Vs EV

This section discusses a comparison between EB and EV. Unlike EV, EB does not have space limitation, which makes the installation of PVs easier. So, EBs can charge their battery and make their power less intermittent. The EVs designed with roof-mounted solar panels face challenges to utilize sunlight due to the shade of buildings, trees, and parking lots. However, PV-attached EB does not face this problem. So, while EBs are at work, they still can charge their batteries. The case study associated with Figure 6 is conducted in this section using EVs as well. A Nissan Leaf EV with 30 kWh battery capacity, $65\% \leq SOC \geq 95\%$ for V2G is used. Alike EB, EV leaves home at 8 am for work (no charging facility at work) and comes back at 3 pm with a daily trip distance between 40- 50 km. Since EV does not have a continuous charging facility, when it comes back home from work at 3 pm its SOC< lower discharging limits, so it takes power from the grid instead of load-support, as shown in Figure 29. On the other hand, EB provides load support immediately after returning home, and it continues throughout the peak periods between 3- 9 pm. So, it is clear from the case study that the load-support by EBs to the grid is higher than the EVs. The contribution by EVs can be enhanced by adding more battery capacity and giving flexibility to discharging boundaries; however, the easy installation of PVs at EB will continue to provide advantages than that of EVs without PVs.

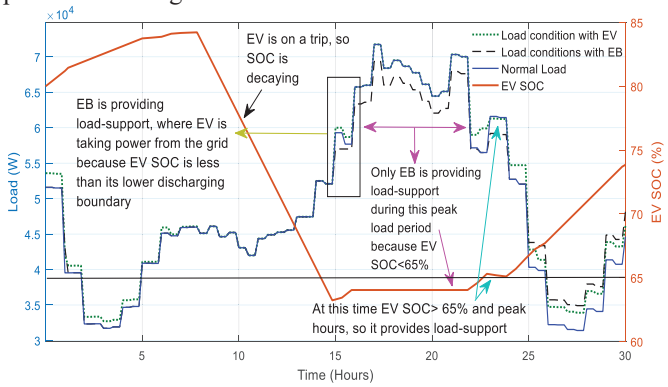

Fig. 29. A comparative performance analysis between EB and EV.

V. Experimental Results

The proposed system is tested in a laboratory-scale microgrid. All the energy sources (PV, EB, battery) and loads are connected to the common bus of this single-phase microgrid. The bus voltage is the standard Australian distribution-side nominal voltage of 230 V. A PV emulator is used to test the real PV power generator. The PV emulator is connected to the common bus through a DC-AC inverter. To emulate the electric boat, 4 gel batteries are used. Each of the batteries is 6 V, and connected in a series to make 24 V. This 24 V DC voltage is stepped up to 230 V AC to connect to the common AC bus. Customers' variable load demand is emulated using a programmable AC load. The overall experimental setup is shown in Figure 30(a). Since the bus

This article has been accepted for publication in a future issue of this journal, but has not been fully edited. Content may change prior to final publication. Citation information: DOI 10.1109/TII.2019.2926511, IEEE Transactions on Industrial Informatics

voltage is constant, current changes are based on the customers' power demand. Thus, the conditions of the current are monitored under various scenarios. In Figure 30(b), customers' current demand is 9.34 A, which is supported by the EB (4.9 A) and PV (3.4 A), and the rest is supported by the community generator.

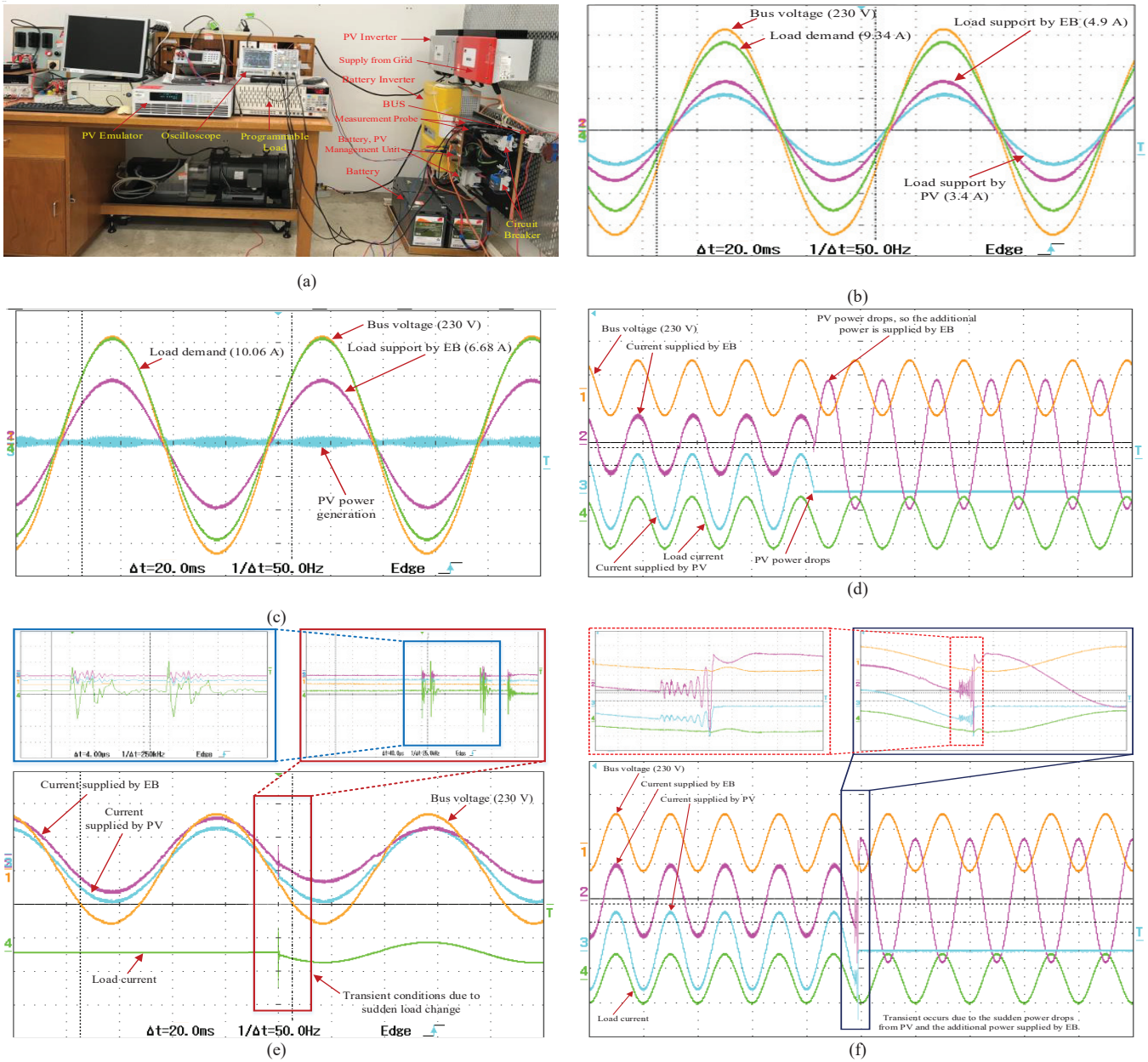

Fig. 30. (a). Experimental setup, (b). load-support using EB, PV and community generator, (c). load-support from EB and community generator in case of PV intermittency, (d). load-support by EB in case of a sudden power source drop, (e). load disturbances and system robustness investigation, (f). system robustness analysis in case of power-source switching.

Since the PV power generation is intermittent, during its limited (or zero) power generation, the customers' demand is supported by the EB and the community generator, as shown in Figure 30(c). If any energy source is disconnected due to its intermittency or constraints, the other available sources support the customers' demand. In Figure 30(d), when PV power generation stops, the available EBs start providing additional power to replace the missing PV power. In case of any disturbances in load or source, the proposed control algorithm shows a robust behavior. In Figure 30(e), a load switching is done to observe the transient in bus voltage, and PV and EB currents. It is found that a small transient occurs in PV and EB currents, but the voltage remains stable. Likewise, a sudden switching was done on the power sources side, as in Figure 30(f). When PV power generation is suddenly disconnected, the additional power is supplied by the EB with a micro-second response, with a very small transient. As the experimental setup is a single-phase system, only sudden interruption of sources/loads was tested and not the three-phase fault conditions.

VI. Conclusion

This paper sets out to provide necessary insights to the energy management of a small remote island using existing

resources such as PV units, battery energy storage systems and EBs. Additionally, it has been one of the first attempts to thoroughly examine the impact of EBs' integration in a small-scale power system to meet customers' energy demand while maintaining power-quality requirements. The studies presented here suggest that proper coordination and management of EBs along with battery storage and PVs can provide a substantial load and ancillary support to the grid. Moreover, the different analyses with various combinations of PV units, EBs and battery energy storage systems under uncertainties and fault conditions suggest that the robust behavior of the proposed method is capable of providing load and ancillary support, and is resilient to any risks. The proposed methodology can be adopted to develop an island energy system reducing the dependency on costly diesel generators. The future aim of this study is to develop an energy management system for industrial customers under unbalanced loading conditions and the use of wind power generator with a combination of EBs.

REFERENCES

[1] Q. Wu, E. Larsen, K. Heussen, H. Binder, and P. Douglass, "Remote Off-Grid Solutions for Greenland and Denmark: Using smart-grid technologies to ensure secure, reliable energy for island power systems," *IEEE Electrification Magazine,* vol. 5, no. 2, pp. 64-73, 2017.

[2] M. H. K. Tushar, C. Assi, "Optimal energy management and marginal-cost electricity pricing in microgrid network," *IEEE Transactions on Industrial Informatics,* vol. 13, no. 6, pp. 3286-3298, 2017.

[3] Y.-K. Wu, "Frequency stability for an island power system: Developing an intelligent preventive-corrective control mechanism for an offshore location," *IEEE Industry Applications Magazine,* vol. 23, no. 2, pp. 74-87, 2017.

[4] H. Khorramdel, J. Aghaei, B. Khorramdel, O. Siano, "Optimal battery sizing in microgrids using probabilistic unit commitment," *IEEE Transactions on Industrical Informatics,* vol. 12, no. 2, pp. 834-843, 2016.

[5] K. Bellache, M. B. Camara, and B. Dakyo, "Transient Power Control for Diesel-generator assistance in Electric Boat Applications using Supercapacitors and Batteries," *IEEE Journal of Emerging and Selected Topics in Power Electronics,* 2017.

[6] Z. Zhou, M. B. Camara, and B. Dakyo, "Coordinated Power Control of Variable-Speed Diesel Generators and Lithium-Battery on a Hybrid Electric Boat," *IEEE Transactions on Vehicular Technology,* vol. 66, no. 7, pp. 5775-5784, 2017.

[7] N. Hatziargyriou, I. Margaris, I. Stavropoulou, S. Papathanassiou, and A. Dimeas, "Noninterconnected Island Systems: The Greek Case," *IEEE Electrification Magazine,* vol. 5, no. 2, pp. 17-27, 2017.

[8] P. Li, R. X. Li, Y. Cao, D. Y. Li, G. Xie, "Multiobjective sizing optimization for island microgrids using a triangular aggregation model and the levy-harmony algorithm," *IEEE Transactions on Industrial Informatics,* vol. 14, no. 8, pp. 3495-3505, 2018.

[9] G. N. Psarros, S. I. Nanou, S. V. Papaefthymiou, and S. A. Papathanassiou, "Generation scheduling in non-interconnected islands with high RES penetration," *Renewable Energy,* vol. 115, pp. 338-352, 2018.

[10] Y. Tian, L. Fan, Y. Tang, K. Wang, G. Li, and H. Wang, "A Coordinated Multi-time Scale Robust Scheduling Framework for Isolated power System with ESU under High RES Penetration," *IEEE Access,* 2018.

[11] S. Gill *et al.*, "Increasing renewable penetration on islanded networks through active network management: a case study from Shetland," *IET Renewable Power Generation,* vol. 9, no. 5, pp. 453-465, 2015.

[12] A. V. Ntomaris and A. G. Bakirtzis, "Stochastic scheduling of hybrid power stations in insular power systems with high wind penetration," *IEEE Transactions on Power Systems,* vol. 31, no. 5, pp. 3424-3436, 2016.

[13] C.-C. Yeh *et al.*, "Design of Special Protection System for an Offshore Island With High-PV Penetration," *IEEE Transactions on Industry Applications,* vol. 53, no. 2, pp. 947-953, 2017.

[14] C. Li *et al.*, "A time-scale adaptive dispatch method for renewable energy power supply systems on islands," *IEEE Transactions on Smart Grid,* vol. 7, no. 2, pp. 1069-1078, 2016.

[15] I. Miranda, N. Silva, and H. Leite, "A holistic approach to the integration of battery energy storage systems in island electric grids with high wind penetration," *IEEE Transactions on Sustainable Energy,* vol. 7, no. 2, pp. 775-785, 2016.

[16] E.-H. Kim, J.-H. Kim, S.-H. Kim, J. Choi, K. Y. Lee, and H.-C. Kim, "Impact analysis of wind farms in the Jeju Island power system," *IEEE Systems Journal,* vol. 6, no. 1, pp. 134-139, 2012.

[17] S. V. Papaefthymiou, E. G. Karamanou, S. A. Papathanassiou, and M. P. Papadopoulos, "A wind-hydro-pumped storage station leading to high RES penetration in the autonomous island system of Ikaria," *IEEE Transactions on Sustainable Energy,* vol. 1, no. 3, pp. 163-172, 2010.

[18] M. Patterson, N. F. Macia, and A. M. Kannan, "Hybrid microgrid model based on solar photovoltaic battery fuel cell system for intermittent load applications," *IEEE Transactions on Energy Conversion,* vol. 30, no. 1, pp. 359-366, 2015.

[19] M. S. Rahman, J. Hossain, J. Lu, and H. R. Pota, "A Need-Based Distributed Coordination Strategy for EV Storages in a Commercial Hybrid AC/DC Microgrid with an Improved Interlinking Converter Control Topology," *IEEE Transactions on Energy Conversion,* 2017.

[20] A. Saad, T. Youssef, A. T. Elsayed, A. Amin, O. H. Abdalla, O. A. Mohammed, "Data-centric hierarchical distributed model predictive control for smart grid energy management," *IEEE Transactions on Industrical Informatics,* 2018.

[21] E. I. Vrettos and S. A. Papathanassiou, "Operating policy and optimal sizing of a high penetration RES-BESS system for small isolated grids," *IEEE Transactions on Energy Conversion,* vol. 26, no. 3, pp. 744-756, 2011.

[22] M. Marchiano, D. Rayworth, E. Alegria, and J. Undrill, "Power Generation Load Sharing Using Droop Control in an Island System," *IEEE Transactions on Industry Applications,* 2017.

[23] Y.-K. Wu, G.-T. Ye, and K.-T. Tang, "Preventive control strategy for an island power system that considers system security and economics," *IEEE Transactions on Industry Applications,* 2017.

[24] J. M. Guerrero, J. C. Vasquez, J. Matas, L. G. d. Vicuna, and M. Castilla, "Hierarchical Control of Droop-Controlled AC and DC Microgrids- A General Approach Toward Standardization," *IEEE Transactions on Industrial Electronics*, vol. 58, no. 1, pp. 158-172, 2011.

[25] A. Yazdani and R. Iravani, *Voltage-sourced converters in power systems: modeling, control, and applications*. John Wiley & Sons, 2010.

[26] N. Mahmud, A. Zahedi, A. Mahmud, "A Cooperative Operation of Novel PV Inverter Control Scheme and Storage Energy Management System Based on ANFIS for Voltage Regulation for Grid-Tied PV System" *IEEE Transactions on Industrial Informatics*, vol. 13, no. 5, pp. 2657-2668, 2017.

[27] K. Mahmud, MJ Hossain, J. Ravishankar, "Peak load management in commercial systems with electric vehicles" *IEEE Systems Journal*, vol. 13, no. 2, pp. 1872-1882, 2019.

[28] MS. Rahman, MJ Hossain, J. Liu, "Coordinated control of three-phase AC and DC type EV-ESSs for efficient hybrid microgrid operations" *Energy Conversions and Management*, vol. 122, pp. 488-503.